THE JOURNAL OF PHYSICAL CHEMISTRY Letters

Letter

pubs.acs.org/JPCL

Impact of Electrocatalyst Activity and Ion Permeability on Water-Splitting Photoanodes

Fuding Lin, Benjamin F. Bachman, and Shannon W. Boettcher*

Department of Chemistry and Biochemistry, Materials Science Institute, University of Oregon, Eugene, Oregon 97403, United States

Supporting Information

ABSTRACT: Electrocatalyst (EC)-modified semiconductor (SC) photoelectrodes are key elements of solar water-splitting systems. The SC|EC interface affects the composite photoelectrode behavior but is poorly understood. We uncover the role of EC activity and SC|EC interface properties using a range of metal (Ni, Fe, Ni–Fe, Co, Ir) oxide or (oxy)hydroxide ECs deposited on model single-crystal n-TiO_2 photoanodes. The impedance and photoelectrochemical response of the system was nearly independent of EC oxygen evolution activity if the catalyst was deposited electrochemically as an ion-permeable (oxy)hydroxide or hydrous oxide. When dense oxides (e.g., ion-impermeable) ECs were used, the response depended strongly on the EC. These data demonstrate that the EC and SC interface structures are more important than the EC activity in determining the composite photoanode response, confirming recent SC|EC interface simulations for ion-permeable ECs. These results thus inform the design of high-performance water-oxidizing photoanodes with direct SC|EC interfaces.

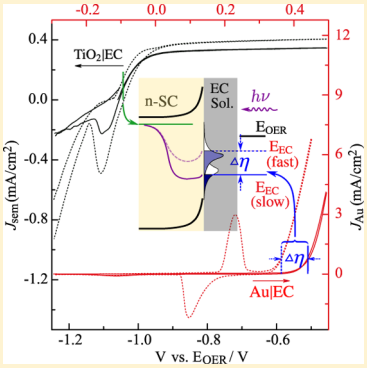

Generating H_2 fuel via solar water splitting provides one strategy to both convert and store solar energy. A key challenge is to develop stable and efficient photoelectrodes for each half reaction that can be used in a tandem water splitting cell,[1] especially for the kinetically slow oxygen evolving reaction (OER). Known semiconductors (SCs) with suitable band gaps and electronic properties for photoanodes (e.g., $BiVO_4$) are not good OER catalysts.[2−4] Therefore, additional materials, that is, electrocatalysts (ECs), are routinely deposited onto light-absorbing SCs to increase kinetics and form a SC|EC composite photoelectrode.[5−9] The properties of the SC|EC interface are not well understood.[3,10,11]

Without an EC layer, the SC forms a SC|solution junction with the contacting electrolyte and the photogenerated charge carriers from the SC drive the OER (or hydrogen evolving reaction (HER)) at the SC surface directly.[1] In this scenario, the isolated Fermi level (E_f) of the SC and the redox energy level (E_{redox}) of the solution determine the built-in potential (V_{bi}) in equilibrium and set the upper limit of the measurable open-circuit potential (V_{oc}) generated by an ideal SC|solution junction under illumination.[12]

Coating the SC with an EC overlayer creates a SC|EC|solution structure that could bring several advantages compared to the simple SC|solution junction, but the interfacial charge-transfer processes are significantly more complicated.[13]

If the EC layer is dense and impermeable to solution, substantial electronic charge cannot accumulate inside of the EC (because it must be screened by ionic charge), and therefore, the difference between the EC Fermi level and the edge of the SC conduction or valence band at the contact interface (i.e., the junction barrier height ϕ_b in Figure 1a) is constant for a given SC–EC pair. The SC|EC|solution system can thus be treated as a solid-state heterojunction (with a constant V_{bi}) in series with the EC|solution interface.[13,14] Such a "buried" SC|EC junction provides several potential performance benefits. First, because V_{bi} is independent of E_{redox}, the solid-state interface can be engineered using traditional techniques used for heterojunction photovoltaics in order to increase the V_{bi} and thus V_{oc} of the buried junction (Figure 1a,b). Second, the EC surface composition can be controlled to minimize the overpotential loses (η in Figure 1b), driving catalysis without concern over the effect on the buried junction performance. Properties of both the SC|EC junction and the catalyst can thus be independently tuned to increase the PEC performance of the composite photoelectrode.[15] Unfortunately, it is not easy to make high-quality buried junctions for many SCs, particularly oxides.

If the EC layer is ion-permeable, as is the case for many hydrous metal oxyhydroxides,[16−18] the entire EC layer is able to undergo oxidation and reduction as electronic charges are injected into or extracted out of the EC.[19] The ion-permeable EC in effect functions as a surface-attached redox system. The bulk oxidation and reduction of the EC shift its Fermi level relative to the SC conduction/valence band edge, resulting in an "adaptive" junction with an effective ϕ_b (and hence V_{bi}) that increases as the EC is oxidized during operation.[20] As shown in Figure 1c,d, the ion permeability of the EC screens electronic charge in the EC bulk and thus requires all of the electrostatic potential to drop across the SC depletion region or interface. The dense EC case is markedly different; a change in the Helmholtz potential at the EC|solution interface V_H^{EC} (Figure

Received: May 1, 2015
Accepted: June 5, 2015
Published: June 5, 2015

DOI: 10.1021/acs.jpclett.5b00904
J. Phys. Chem. Lett. 2015, 6, 2427−2433

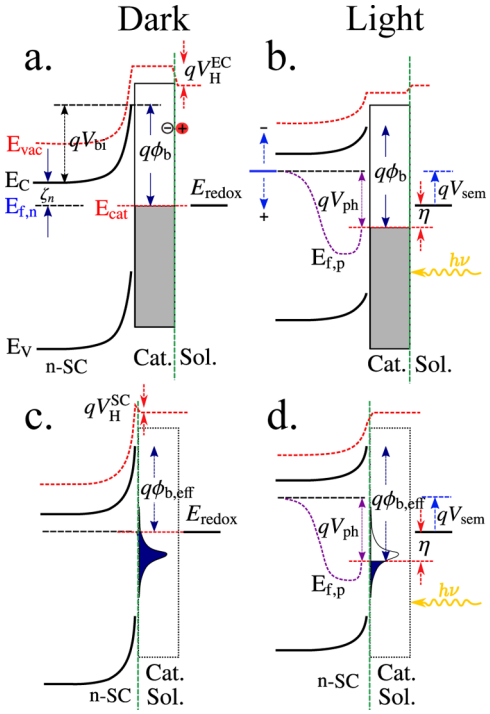

Figure 1. Energy level diagram for composite photoanodes. (a) Dense catalyst overlayer at dark equilibrium and (b) illuminated. (c) Ion-permeable catalyst at dark equilibrium and (d) illuminated. E_{vac} is the vacuum energy level referenced to the charge-neutral solution; E_{redox} is the Fermi level of the solution species, that is, the thermodynamic redox potential of OER at a given pH (E_{OER}). E_{cat} is the Fermi level of the EC. $E_{f,n}$ and $E_{f,p}$ are quasi-Fermi level of electrons and holes, respectively, in the SC. E_C and E_V are the SC conduction and valence band edge energies, respectively. ϕ_b is the separation between the SC conduction band edge energy and the EC Fermi level at the SC|EC interface. V_H^{EC} and V_H^{SC} are the Helmholtz potential difference across the EC|solution and the SC|solution interfaces, respectively. V_{sem} is the measured (or applied) potential at the SC ohmic back contact referenced to E_{redox}. Other variables are defined as shown in the diagram. For ion-permeable ECs (bottom), ϕ_b effectively increases under illumination, whereas for the dense ECs (top), ϕ_b remains constant.[13] In (a) and (b), the dense EC electronic structure is depicted as a metal, while in (c) and (d), the ion-permeable structure is shown with a narrower band more appropriate for a surface-attached redox system to highlight possible differences between the two. However, the details of the EC electronic structure (metal, doped SC, surface-attached redox system) are secondary to the question of ion permeability considered here.

1a,b) is necessary to drive OER, leading to a shift in the absolute SC band edge position.

We have previously demonstrated experimentally the sharp contrast between the nonequilibrium photovoltage output (V_{ph} in Figure 1b,d) of a buried junction and an adaptive junction using dense IrO_x and ion-permeable $Ni(OH)_2$/NiOOH, respectively, as two representative ECs.[20]

However, at equilibrium (Figure 1c), the ϕ_b of a junction between the SC and ion-permeable EC is predicted to be similar to that of a SC|solution junction if the EC Fermi level is determined by the solution that permeates throughout the EC layer. In this case, V_{fb} measured through electrochemical impedance spectroscopy (EIS), which is typically performed in the dark, will not reflect changes in the effective ϕ_b when the junction is illuminated. Furthermore, because V_{fb} is measured against the reference electrode (and thus E_{redox}), only changes in the Helmholtz potential difference across the SC|solution interface (V_H^{SC})[21] should cause a shift in V_{fb} for a given SC. For ion-permeable ECs, changes in the surface charge at the EC|solution interface are not predicted to lead to changes in V_{fb} because this dipole would simply be screened by electrolyte ions. V_H^{EC} is therefore expected to be nonzero only for the case of dense catalyst, as shown in Figure 1.

The ion-permeable EC, however, might affect the density and/or occupancy of SC surface states or the SC surface dipole V_H^{SC} associated with specifically adsorbed charge, thus affecting indirectly the junction properties and photoelectrode performance. A favorable shift of the SC band edge positions was recently suggested by Choi and co-workers for FeOOH/NiOOH deposited on $BiVO_4$.[9]

Both ion-permeable and dense ECs would be traditionally expected to improve the photoelectrode performance, compared to the uncatalyzed photoelectrode, by increasing reaction kinetics. However, numerical simulations of SC|EC|solution systems show that for a SC with a valence band edge substantially more positive than E_{OER}, the EC activity has essentially no effect on the photoelectrode response over a large activity range.[13] This simulated behavior has been explained by the adaptive SC|EC junction concept, where under operation, the slower ECs are oxidized to a higher level and thus generate a larger effective interface barrier and a junction that provides a larger photovoltage.[20] Another way to describe this phenomenon is that the band edges of the SC remain fixed as charge accumulates in the EC (thus increasing the chemical potential of the EC and providing for the kinetic overpotential) because the electronic charge is screened by electrolyte ions and V_H^{EC} = 0. The increased overpotential required for slower ion-permeable ECs is therefore compensated for by the in situ increase in photovoltage, and the net result is a reduced dependence of photoelectrode performance on EC activity.

Experimental evidence for this type of adaptive junction has been obtained using the dual-electrode photoelectrochemistry technique for the test case of ion-permeable NiOOH EC layers.[20]

The reduced impact of ion-permeable EC activity on composite photoelectrode performance predicted by the adaptive junction model points to a new design principle for PEC devices. Experimental verification of these predictions is important. The impact of EC activity on photoelectrode response in either the dense or the ion-permeable cases has not been studied in a controlled way. This experiment is challenging because the impact of EC activity is often convolved with other effects brought about by the EC, such as SC surface state modification and induced SC band edge shifts.

In order to demonstrate the impact of catalyst activity in either the "buried" or the "adaptive" junction case, it is necessary to use catalysts that are different in activity but similar in all other aspects. In the buried junction case, we used spin coating followed by thermal decomposition (see the Supporting Information (SI) for details) to deposit thin-film oxides of Co, Ni, Fe, and Ir onto both single-crystal n-TiO_2 and conductive indium tin oxide (ITO), or Au/Ti, on glass substrates. We then measured composite photoanode response along with the OER activity of each oxide on the conductive support. The materials characterization of ECs prepared in this way has been reported previously.[16]

DOI: 10.1021/acs.jpclett.5b00904
J. Phys. Chem. Lett. 2015, 6, 2427−2433

Repetitive voltage cycling of thermally deposited oxide catalysts on an ITO substrate dramatically affects the OER activity of both the Ni and Ir oxides, while that of the CoO_x and FeO_x films is relatively unchanged (Figure 2a). The quantitative

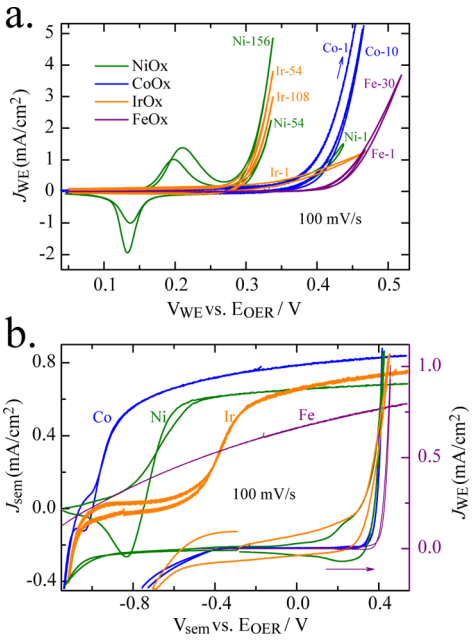

Figure 2. PEC performance of n-TiO_2 photoanodes with thermally deposited metal oxide catalysts. (a) Changes in OER activity and redox capacity of thermally deposited oxide catalyst films on ITO substrates after repetitive redox cycling in 0.1 M KOH at 100 mV/s. The scan cycle shown is indicated in the curve label. V_{WE} is the potential of the conductive substrate in contact with the EC. (b) The cyclic voltammogram of n-TiO_2|EC junctions under 1 sun illumination at 100 mV/s, shown with the initial OER activity of dense catalysts on a conductive substrate, replotted from panel (a).

conversion of dense nanocrystalline NiO_x into ion-permeable NiOOH accompanied by the incorporation of Fe solution impurities has been well documented and explains the observed behavior including the growth of the reversible redox wave prior to the OER onset.[16] For IrO_x, we observe a factor of 2 increase in the pseudocapacitance up to 54 cycles, which is consistent with an increase in the effective surface area and a partial conversion to the hydrous oxide. This is followed by a decrease in activity and pseudocapactiance for longer cycling associated with dissolution of the IrO_x in KOH.[22,23] Although the Co catalyst initially appears to be more active than both the Ni and the Ir catalysts, it is outperformed substantially once the Ni and Ir oxide films are activated upon cycling.

The activity and redox capacity changes of a dense EC upon repetitive cycling could impact the PEC response of the EC-coated n-TiO_2. The illuminated J–E curve of FeO_x- or CoO_x-coated photoanodes, however, did not change with cycling, consistent with their stable activity and redox capacitance on conductive substrates. Although the IrO_x showed growing pseudocapacitance with cycling, the PEC behavior of n-TiO_2|IrO_x did not change initially and only changed substantially after extended cycling and dissolution of the IrO_x. In contrast, the PEC response of n-TiO_2|NiO_x steadily improved with cycling until both activity and redox capacity stabilized. This suggests that the electrolyte did not come into contact with n-TiO_2 until the entire IrO_x film was hydrated, but that electrolyte permeated through the NiO_x film almost immediately upon cycling.

To best represent the buried junction scenario, only the first scans of both the dark OER activity and the illuminated J–E curves are compared in Figure 2b. While the photocurrent onset potentials differ by over 600 mV for the different samples, the initial OER onset potentials differ by <50 mV at 0.5 mA/cm^2. Furthermore, the sample with FeO_x shows an extremely poor fill factor, likely related to the low conductivity of FeO_x.[24] The dramatic differences in photocurrent onset thus cannot be explained by differences in EC activity and must be due to differences in the buried SC|EC heterojunction. It is interesting to note that the best buried junction is formed by CoO_x, which is known to exhibit p-type conductivity and thus perhaps form a reasonable pn heterojunction with n-TiO_2.[25,26] A previous study has shown that similarly deposited CoO_x films appears to be crystalline in structure and only about 4% of the film mass is redox-active, which suggest that the bulk of the CoO_x film is not permeable to the electrolyte.[16] However, it is still possible that the n-TiO_2 surface is not completely covered by CoO_x, and the presence of a mixed solution/solid-state junction might contribute to the better apparent performance compared to the other dense EC films.

To further investigate the SC|EC interface for the thermally deposited "dense" ECs, we used impedance spectroscopy. The data were modeled with an $R_s + R_p/C_p$ circuit to extract the apparent depletion capacitance as a function of applied potential. A comparison of the modeled and measured impedance spectroscopy data can be found in Figure S1 (SI). The resulting Mott–Schottky data (as shown in Figure 3) were apparently complicated by differences in catalyst conductivity and SC|EC interface energetics. For example, the capacitance of

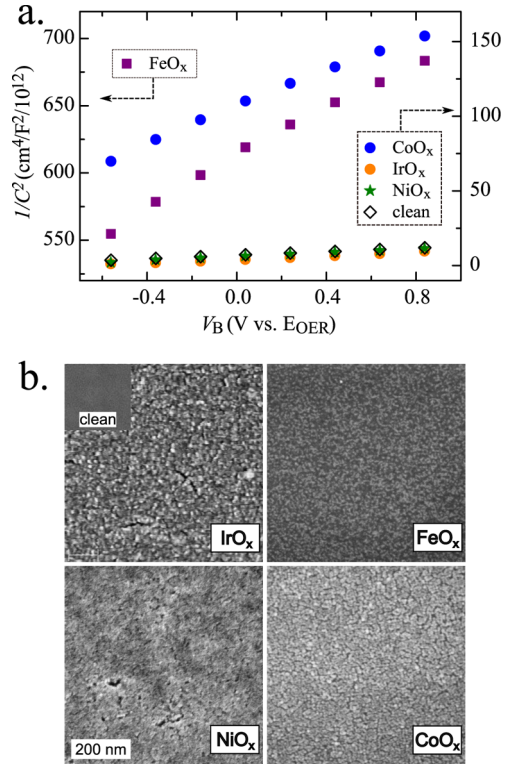

Figure 3. (a) Mott–Schottky data of n-TiO_2 photoanodes with and without thermally deposited Ir, Fe, Ni, and Co oxide ECs and (b) SEM images of each catalyst film on n-TiO_2.

DOI: 10.1021/acs.jpclett.5b00904
J. Phys. Chem. Lett. 2015, 6, 2427–2433

the FeO_x-coated sample is substantially smaller and shows much weaker bias dependence than the others, presumably due to low conductivity of the FeO_x layer. It is therefore difficult to extract and compare V_{fb} values for these samples. Nevertheless, the substantial diversity of the Mott−Schottky intercepts and slopes suggests that equilibrium band bending and SC|EC interface differ significantly among these samples.

As the NiO_x catalyst evolves during cycling and converts to $Ni(OH)_2$/NiOOH,[16] both $J-E$ and impedance data collected throughout the process also changed (Figure 4). The apparent

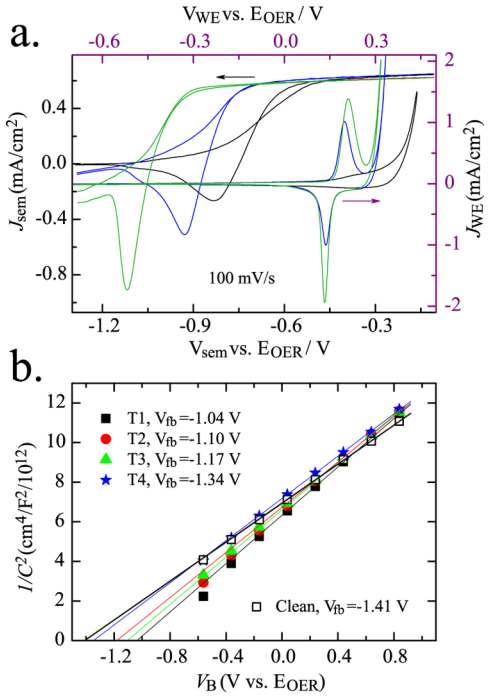

Figure 4. Changes in n-TiO_2|NiO_x junction properties due to hydration of a dense NiO_x film in 0.1 M KOH. (a) Changes in the voltammetry of the n-TiO_2|NiO_x junction under 1 sun illumination and the ITO|NiO_x electrode in the dark upon repetitive cycling at a scan rate of 100 mV/s. (b) Changes in capacitance−voltage response of a n-TiO_2|NiO_x junction during the hydration process showing a gradual negative shift in V_{fb}. Data from a clean n-TiO_2 sample is also shown for reference. Labels T1−T4 represent increasing time during the conditioning process.

V_{fb} (Figure 4b) increased from −1.04 to −1.34 V, consistent with hydration of the EC allowing electrolyte to permeate to the SC surface. We note also that the slope of the Mott−Schottky plot changes slightly during the conversion. Given that the dopant density in the n-TiO_2 is unlikely to change, we attribute this to interface modifications upon hydration that are not captured by the simple equivalent circuit used. We discuss the impedance of the SC|EC junction with ion-permeable catalysts in greater detail below.

For the PEC $J-E$ curves, the cathodic shift of the photocurrent onset (increased V_{oc}) for n-TiO_2|NiO_x upon NiO_x hydration correlates well with the increase in redox capacity and apparent OER activity on ITO substrates (Figure 4a). Although it is reasonable to assume that both increased activity and the gradual transition to an "adaptive" junction contribute to the performance increase, separating the contributions of each mechanism is difficult.

To study the effect of EC activity alone, we next used ECs that are all ion-permeable. Common ECs, including $Ni(OH)_2$/NiOOH, FeOOH, CoOOH, and $IrO_x{\cdot}xH_2O$, can be electrodeposited as hydroxides, oxyhydroxides, or hydrous oxides directly on the SC surface and tested without drying or heating.[9,27,28] Catalysts prepared by such methods exhibit a range of OER activity and appear ion-permeable based on voltammetric and impedance analysis.[29−32] Discussion of the evidence supporting ion permeability is included in the SI (also see Table S1 and Figure S3). If these catalysts result in adaptive SC|EC junctions when deposited on n-TiO_2, simulations predict that the illuminated $J-E$ curves will have minimal dependence on the catalyst activity, unless deposition accompanies substantial changes to V_{fb} due to a dipole at the SC surface affecting V_H^{SC}.

To test these predictions, each EC was electrodeposited onto both conductive Au/Ti/glass and single-crystal n-TiO_2 substrates. Because all of the electrodeposited ECs, with the exception of the hydrous IrO_x, are acid-soluble and thus easily removed from the n-TiO_2 with 2 M HCl, we used the same n-TiO_2 substrate to conduct experiments with all ECs. This approach has the advantage of minimizing the variation in $J-E$ response due to differences among n-TiO_2 substrates. Cyclic voltammograms of the n-TiO_2|EC samples under 1 sun illumination and the control EC samples on conductive substrates (in the dark) are shown in Figure 5a. Similar results were obtained when the experiments were repeated with other n-TiO_2 substrates and with different orders of EC deposition.

The OER "onset" potentials for the ECs on Au differ by ∼130 mV at 1.0 mA/cm^2 (Figure 5a). When the same ECs were deposited onto n-TiO_2, all composite photoanodes exhibited nearly identical photocurrent onset potentials (within error). The spread in voltage at the maximum power point among all samples shown in Figure 5a is ∼30 mV. The variation in short-circuit current among the four SC|EC samples was due to differences in parasitic optical absorption by each EC film.[33] The SC|EC composite devices also show different degrees of hysteresis near the photocurrent onset, which is associated with the faradaic charging and discharging of the catalyst. SEM imaging of the composite electrodes confirm uniform coverage of the n-TiO_2 (Figure 5b).

The minimal effect of catalytic activity on overall SC|EC photoanode performance is consistent with the formation of adaptive SC|EC junctions due to ion permeability of the electrochemically deposited catalyst film and with previous $J-E$ curves from simulation.[13] For a SC with a deep valence band edge (i.e., more oxidizing than the thermodynamic OER potential E_{redox} by more than the OER overpotential of the given EC at the operational photocurrent density), as in the case of n-TiO_2, the activity difference among the ECs becomes less important because the in situ effective barrier height simply increases more for worse ECs. Because depositing an ion-permeable catalyst layer on the SC does not prevent the SC from directly contacting the solution, it is in principle possible for the holes to bypass the EC and directly pass to the solution. Our previous work, however, has demonstrated that holes pass through the EC instead of directly oxidizing water on the n-TiO_2 surface.[20] This is explained by the faster kinetics for one-electron redox activity of the transition-metal EC layer compared to the slower four-electron water oxidation kinetics directly on n-TiO_2 (see additional discussion in the SI).

It is also possible that catalyst-induced flat-band potential (V_{fb}) shifts, as suggested by Choi and co-workers for FeOOH/

DOI: 10.1021/acs.jpclett.5b00904
J. Phys. Chem. Lett. 2015, 6, 2427−2433

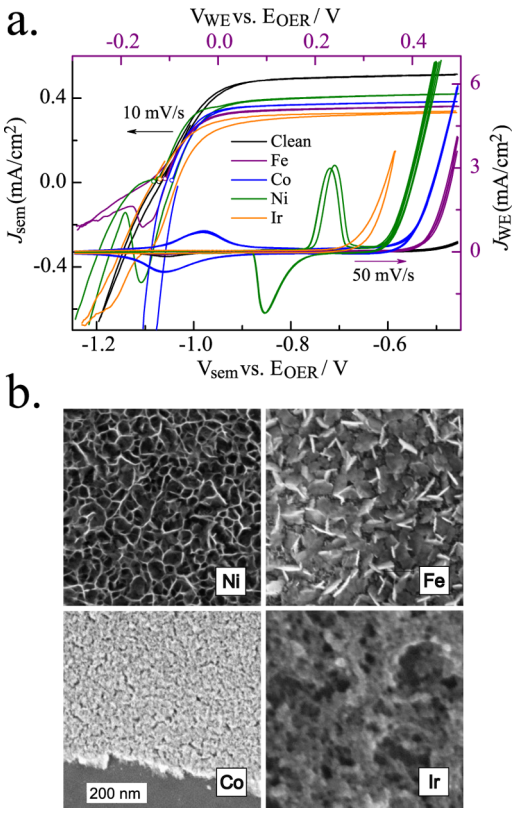

Figure 5. (a) The cyclic voltammogram of n-TiO_2|EC junctions with different ion-permeable ECs under 1 sun illumination at a scan rate of 10 mV/s and for each catalyst on conductive substrates in the dark at 50 mV/s. Each CV scan starts from the open-circuit potential, as indicated by a circle, and first scans anodically. The electrolyte was 0.1 M KOH. (b) SEM images of electrochemically deposited Ni, Fe, Co, and Ir oxides/(oxy)hydroxides on n-TiO_2. The NiOOH catalyst here has accumulated some Fe impurities, leading to the relatively high OER activity.[29] For the CoOOH sample, a portion of the film was removed to provide contrast between the n-TiO_2 and catalyst layers.

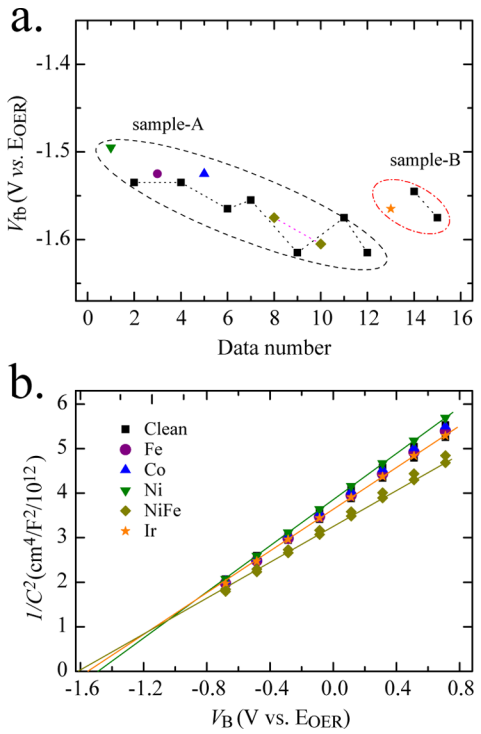

Figure 6. (a) Changes in the extracted V_{fb} in 0.1 M KOH of two n-TiO_2 electrodes with (colored symbols with the legend below) and without (black squares) ion-permeable ECs on the surface. A 2 M HCl solution was used to clean off Ni, Ir, or Co ECs before subsequent deposition of the same or a different material. The data number indicates the sequential order of each Mott−Schottky measurement. Data from the same catalyst but deposited at different times were represented by the same color. (b) The corresponding Mott−Schottky data of (a).

NiOOH on $BiVO_4$, also contribute to the minimal dependence on catalytic activity. To study this, we extracted V_{fb} for n-TiO_2 with each EC via Mott−Schottky analysis (Figure 6a). The n-TiO_2 with ion-permeable ECs exhibited purely capacitive impedance response within a large frequency range (see Figure S1, SI) and thus yielded largely ideal Mott−Schottky plots.

Data in Figure 6a were collected using two similar n-TiO_2 substrates, either with or without an electrochemically deposited catalyst. The corresponding Mott−Schottky data are shown in Figure 6b. The data number indicates the sequential order of each Mott−Schottky measurement.

Within experimental uncertainty of $\Delta V_{fb} \approx 34$ mV, estimated from multiple measurements of sample A, we find no evidence for catalyst-induced V_{fb} shifts (Figure 6a). However, the V_{fb} data does exhibit a cathodic shift with the number of cleaning cycles (see also Figure S2, SI) even though the photocurrent onset of the illuminated J−E curves did not improve. The causes for this V_{fb} shift are not known, but specific adsorption of chloride anions into a hydrated surface layer during cleaning of the n-TiO_2 crystal may contribute. The iron impurities commonly found in an electrochemical cell (see below) could also deposit on the electrode surface and induce changes to V_{fb} that are difficult to control. Polishing the n-TiO_2 surface with a 30 nm diameter colloidal silica suspension on a felt mat returns V_{fb} to near its initial value but requires disassembly of the electrode and induces more uncertainty in V_{fb}.

At this point, it is useful to contrast the J−E response of n-TiO_2 with ion-permeable and dense forms of the same ECs. In particular, IrO_x shows dramatic differences, with the dense EC yielding devices with very low V_{oc} (i.e., a more anodic photocurrent onset potential) compared with $IrO_x{\cdot}xH_2O$ electrodeposited from a colloid suspension. We note that the observed differences are much too large to be attributed to differences in the EC reactive surface area or intrinsic activity of the hydrous versus the oxide phases. This is consistent with the findings by Spurgeon et al. that, when deposited on WO_3, thin but dense IrO_x films created low-barrier SC|EC junctions and led to poor performance while thick but porous IrO_x films yielded the best-performing composite photoanode.[34] Others also found substantial improvement in photoanode performance when $IrO_x{\cdot}xH_2O$ is electrodeposited as (presumably) porous/ion-permeable films.[28,35]

In a final set of experiments, we exploited the fact that the OER activity of NiOOH depends sensitively on the Fe impurity content, which can be changed in situ.[29] This Fe originates from any electrolytes that are not specially purified. We use this phenomenon to isolate the effect of EC activity on the SC|EC response for a single device, thus controlling possible differences in interface passivation as well as any possible dependence on catalyst thickness among the different transition-metal catalysts.[36]

DOI: 10.1021/acs.jpclett.5b00904
J. Phys. Chem. Lett. 2015, 6, 2427−2433

We first electrodeposited $Ni(OH)_2$/NiOOH on a Au substrate without Fe and measured the OER activity of the catalyst film periodically while the film was kept in a fused silica PEC cell containing 0.1 M KOH that had been purified to remove Fe impurities.[29] The trace Fe released from etching of the silica is apparently sufficient to substantially enhance the $Ni(OH)_2$/NiOOH OER activity over the course of several hours (Figure 7).

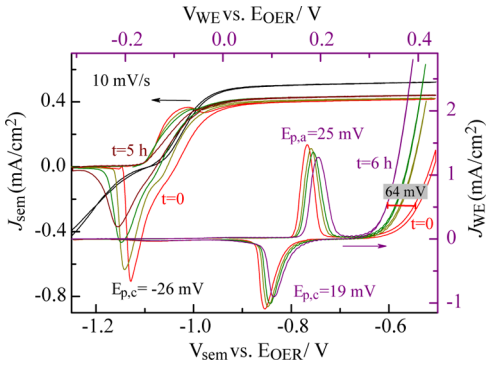

Figure 7. Changes in voltammetry for the *n*-TiO_2|$Ni(OH)_2$/NiOOH junction under 1 sun illumination and the Au|$Ni(OH)_2$/NiOOH electrode in the dark as Fe is absorbed into the anodically deposited, ion-permeable $Ni(OH)_2$/NiOOH film. All data were collected at the same scan rate of 10 mV/s in Fe-free (initially) 0.1 M KOH.

Fe-free $Ni(OH)_2$/NiOOH was then electrodeposited onto a clean *n*-TiO_2 substrate and the *J*−*E* response measured periodically over several hours in the same fused silica cell, with fresh 0.1 M KOH (Fe-free) electrolyte. The results for anodically deposited $Ni(OH)_2$/NiOOH on *n*-TiO_2 are shown in Figure 7. The amount of absorbed Fe in the $Ni(OH)_2$/NiOOH film after cycling is estimated to be 5−10% (total metals basis) from the well-established correlation between redox peak position and Fe content.[27,29]

The composite photoanode shows no change in the photocurrent onset potential at −1.11 V vs E_{OER} measured during the anodic sweep throughout the ∼5 h experiment. Because analysis of the maximum power points of the illuminated *J*−*E* curves were complicated by the redox waves of the EC, we use the potential at which the anodic photocurrent decreases to 90% of the light-limited value at $V_{sem} \approx 0.8$ V to track the PEC performance change. Over the ∼5 h duration, this potential shifted by about −20 mV. As indicated by the experiment conducted on Au, the time was sufficient for the catalyst overpotential to decrease by ∼64 mV at 0.5 mA/cm^2. Because the slow addition of a few percent Fe into the NiOOH film is unlikely to substantially affect the SC|EC interface (i.e., through changes in interface bonding, passivation, or surface dipole) while substantially changing the activity, these results further demonstrate that for ion-permeable catalysts, the EC activity has a reduced impact on the photoelectrochemical response of oxide SCs with deep valence bands, such as *n*-TiO_2.

While both the oxidation and the reduction waves of $Ni(OH)_2$/NiOOH show an anodic shift with increasing Fe absorption when deposited on a conductive Au substrate, the reduction peak shifted in the opposite direction (cathodically) when the EC was deposited on *n*-TiO_2. This could be due to a decrease in the forward electron rate constant for transfer from the conduction band to the empty EC states with an increase in Fe caused by the EC states moving down (more anodic) in energy and thus providing a larger driving force in the Marcus inverted regime.[37] This phenomenon merits further study.

In conclusion, we demonstrated how the activity of ion-permeable ECs affects the performance of composite SC|EC photoelectrodes and found a large difference between dense and ion-permeable ECs. For ion-permeable catalysts, a substantial change in activity does not lead to a commensurate change in SC|EC photoelectrode performance. Further, no evidence of an EC-induced flat-band potential shift was observed when ion-permeable ECs were used on *n*-TiO_2. Dipoles/charges that might be associated with the EC are likely screened by the electrolyte. The diminished impact of EC activity for ion-permeable catalysts is consistent with the formation of an adaptive SC|EC junction, where the in situ change in barrier height ϕ_b compensates for the activity difference. These findings suggest that an effective EC for solar water splitting does not need to be highly active if it is ion-permeable and the SC has a valence band substantially deeper than E_{OER}. For SCs with higher valence bands closer to E_{OER} and/or those whose photovoltage is limited by bulk recombination and not ϕ_b, EC activity is expected to be of more significance. Further study of such systems is still needed to quantitatively test these predictions.

■ ASSOCIATED CONTENT

Supporting Information

Details of sample fabrication, experimental setup, data analysis, additional experiment results regarding the extracted V_{fb}, and supplemental discussion. The Supporting Information is available free of charge on the ACS Publications website at DOI: 10.1021/acs.jpclett.5b00904.

■ AUTHOR INFORMATION

Corresponding Author

*E-mail: swb@uoregon.edu. Phone: +1 541-346-2543.

Notes

The authors declare no competing financial interest.

■ ACKNOWLEDGMENTS

This material is based upon work supported by the U.S. Department of Energy, Office of Science, Office of Basic Energy Sciences, under Award Number DE-FG0212ER16323, and by the Oregon BEST Proposal Matching Grants Program. S.W.B. acknowledges support as a Cottrell Scholar from the Research Corporation for Scientific Advancement. The authors thank Thomas J. Mills for helpful discussions and acknowledge CAMCOR and SuNRISE photovoltaic laboratories for equipment support.

■ REFERENCES

(1) Walter, M.; Warren, E.; McKone, J.; Boettcher, S. W.; Qixi, M.; Santori, L.; Lewis, N. S. Solar Water Splitting Cells. *Chem. Rev.* **2010**, *110*, 6446−6473.

(2) Park, Y.; McDonald, K. J.; Choi, K. S. Progress in Bismuth Vanadate Photoanodes for Use in Solar Water Oxidation. *Chem. Soc. Rev.* **2013**, *42*, 2321−2337.

(3) Sivula, K. Metal Oxide Photoelectrodes for Solar Fuel Production, Surface Traps, and Catalysis. *J. Phys. Chem. Lett.* **2013**, *4*, 1624−1633.

(4) Liang, Y. Q.; Tsubota, T.; Mooij, L. P. A.; van de Krol, R. Highly Improved Quantum Efficiencies for Thin Film $BiVO_4$ Photoanodes. *J. Phys. Chem. C* **2011**, *115*, 17594−17598.

DOI: 10.1021/acs.jpclett.5b00904
J. Phys. Chem. Lett. 2015, 6, 2427−2433

(5) Abdi, F. F.; Firet, N.; van de Krol, R. Efficient $BiVO_4$ Thin Film Photoanodes Modified with Cobalt Phosphate Catalyst and W-Doping. *ChemCatChem* **2013**, *5*, 490−496.
(6) Berglund, S. P.; Flaherty, D. W.; Hahn, N. T.; Bard, A. J.; Mullins, C. B. Photoelectrochemical Oxidation of Water Using Nanostructured $BiVO_4$ Films. *J. Phys. Chem. C* **2011**, *115*, 3794−3802.
(7) Seabold, J. A.; Choi, K. S. Efficient and Stable Photo-Oxidation of Water by a Bismuth Vanadate Photoanode Coupled with an Iron Oxyhydroxide Oxygen Evolution Catalyst. *J. Am. Chem. Soc.* **2012**, *134*, 2186−2192.
(8) Zhong, D. K.; Choi, S.; Gamelin, D. R. Near-Complete Suppression of Surface Recombination in Solar Photoelectrolysis by "Co-Pi" Catalyst-Modified W:$BiVO_4$. *J. Am. Chem. Soc.* **2011**, *133*, 18370−18377.
(9) Kim, T. W.; Choi, K. S. Nanoporous $BiVO_4$ Photoanodes with Dual-Layer Oxygen Evolution Catalysts for Solar Water Splitting. *Science* **2014**, *343*, 990−994.
(10) Gamelin, D. R. Water Splitting Catalyst or Spectator? *Nat. Chem.* **2012**, *4*, 965−967.
(11) Peter, L. M.; Wijayantha, K. G. U. Photoelectrochemical Water Splitting at Semiconductor Electrodes: Fundamental Problems and New Perspectives. *ChemPhysChem* **2014**, *15*, 1983−1995.
(12) Practically the solution potential may not be well defined if the redox kinetics are slow (e.g., water oxidation) and the actual extent of dark equilibrium band bending could also be affected by trace impurities. Therefore, V_{bi} is experimentally inferred from the value of the flat-band potential (V_{fb}) obtained through EIS and referenced to a thermodynamic potential such as that of a reversible hydrogen (or oxygen) electrode.
(13) Mills, T. J.; Lin, F. D.; Boettcher, S. W. Theory and Simulations of Electrocatalyst-Coated Semiconductor Electrodes for Solar Water Splitting. *Phys. Rev. Lett.* **2014**, *112*, 148304.
(14) Winkler, M. T.; Cox, C. R.; Nocera, D. G.; Buonassisi, T. Modeling Integrated Photovoltaic−Electrochemical Devices Using Steady-State Equivalent Circuits. *Proc. Natl. Acad. Sci. U.S.A.* **2013**, *110*, E1076−E1082.
(15) Hu, S.; Shaner, M. R.; Beardslee, J. A.; Lichterman, M.; Brunschwig, B. S.; Lewis, N. S. Amorphous TiO_2 Coatings Stabilize Si, GaAs, and GaP Photoanodes for Efficient Water Oxidation. *Science* **2014**, *344*, 1005−1009.
(16) Trotochaud, L.; Ranney, J. K.; Williams, K. N.; Boettcher, S. W. Solution-Cast Metal Oxide Thin Film Electrocatalysts for Oxygen Evolution. *J. Am. Chem. Soc.* **2012**, *134*, 17253−17261.
(17) McAlpin, J. G.; Stich, T. A.; Casey, W. H.; Britt, R. D. Comparison of Cobalt and Manganese in the Chemistry of Water Oxidation. *Coord. Chem. Rev.* **2012**, *256*, 2445−2452.
(18) Doyle, R. L.; Lyons, M. E. G. An Electrochemical Impedance Study of the Oxygen Evolution Reaction at Hydrous Iron Oxide in Base. *Phys. Chem. Chem. Phys.* **2013**, *15*, 5224−5237.
(19) Wehrens-Dijksma, M.; Notten, P. H. L. Electrochemical Quartz Microbalance Characterization of $Ni(OH)_2$-Based Thin Film Electrodes. *Electrochim. Acta* **2006**, *51*, 3609−3621.
(20) Lin, F. D.; Boettcher, S. W. Adaptive Semiconductor/Electrocatalyst Junctions in Water-Splitting Photoanodes. *Nat. Mater.* **2014**, *13*, 81−86.
(21) Bisquert, J.; Cendula, P.; Bertoluzzi, L.; Gimenez, S. Energy Diagram of Semiconductor/Electrolyte Junctions. *J. Phys. Chem. Lett.* **2014**, *5*, 205−207.
(22) Hackwood, S.; Dayem, A. H.; Beni, G. Amorphous-Nonmetal to Crystalline-Metal Transition in Electrochromic Iridium Oxide-Films. *Phys. Rev. B* **1982**, *26*, 471−478.
(23) Burke, L. D.; Scannell, R. A. An Investigation of Hydrous Oxide-Growth on Iridium in Base. *J. Electroanal. Chem.* **1984**, *175*, 119−141.
(24) Shinar, R.; Kennedy, J. H. Photoactivity of Doped α-Fe_2O_3 Electrodes. *Sol. Energy Mater.* **1982**, *6*, 323−335.
(25) Kadam, L. D.; Patil, P. S. Thickness-Dependent Properties of Sprayed Cobalt Oxide Thin Films. *Mater. Chem. Phys.* **2001**, *68*, 225−232.
(26) Shinde, V. R.; Mahadik, S. B.; Gujar, T. P.; Lokhande, C. D. Supercapacitive Cobalt Oxide (Co_3O_4) Thin Films by Spray Pyrolysis. *Appl. Surf. Sci.* **2006**, *252*, 7487−7492.
(27) Louie, M. W.; Bell, A. T. An Investigation of Thin-Film Ni−Fe Oxide Catalysts for the Electrochemical Evolution of Oxygen. *J. Am. Chem. Soc.* **2013**, *135*, 12329−12337.
(28) Tilley, S. D.; Cornuz, M.; Sivula, K.; Grätzel, M. Light-Induced Water Splitting with Hematite: Improved Nanostructure and Iridium Oxide Catalysis. *Angew. Chem., Int. Ed.* **2010**, *49*, 6405−6408.
(29) Trotochaud, L.; Young, S. L.; Ranney, J. K.; Boettcher, S. W. Nickel−Iron Oxyhydroxide Oxygen-Evolution Electrocatalysts: The Role of Intentional and Incidental Iron Incorporation. *J. Am. Chem. Soc.* **2014**, *136*, 6744−6753.
(30) Burke, M. S.; Kast, M. G.; Trotochaud, L.; Smith, A. M.; Boettcher, S. W. Cobalt−Iron (Oxy)hydroxide Oxygen Evolution Electrocatalysts: The Role of Structure and Composition on Activity, Stability, and Mechanism. *J. Am. Chem. Soc.* **2015**, *137*, 3638−3648.
(31) Nakagawa, T.; Bjorge, N. S.; Murray, R. W. Electrogenerated IrO_x Nanoparticles as Dissolved Redox Catalysts for Water Oxidation. *J. Am. Chem. Soc.* **2009**, *131*, 15578−15579.
(32) Nakagawa, T.; Beasley, C. A.; Murray, R. W. Efficient Electro-Oxidation of Water near Its Reversible Potential by a Mesoporous IrO_x Nanoparticle Film. *J. Phys. Chem. C* **2009**, *113*, 12958−12961.
(33) Trotochaud, L.; Mills, T. J.; Boettcher, S. W. An Optocatalytic Model for Semiconductor−Catalyst Water-Splitting Photoelectrodes Based on In Situ Optical Measurements on Operational Catalysts. *J. Phys. Chem. Lett.* **2013**, *4*, 931−935.
(34) Spurgeon, J. M.; Velazquez, J. M.; McDowell, M. T. Improving O_2 Production of WO_3 Photoanodes with IrO_2 in Acidic Aqueous Electrolyte. *Phys. Chem. Chem. Phys.* **2014**, *16*, 3623−3631.
(35) Badia-Bou, L.; Mas-Marza, E.; Rodenas, P.; Barea, E. M.; Fabregat-Santiago, F.; Gimenez, S.; Peris, E.; Bisquert, J. Water Oxidation at Hematite Photoelectrodes with an Iridium-Based Catalyst. *J. Phys. Chem. C* **2013**, *117*, 3826−3833.
(36) Carroll, G. M.; Zhong, D. K.; Gamelin, D. R. Mechanistic Insights Into Solar Water Oxidation by Cobalt-Phosphate-Modified α-Fe_2O_3 Photoanodes. *Energy Environ. Sci.* **2015**, *8*, 577−584.
(37) Hamann, T. W.; Gstrein, F.; Brunschwig, B. S.; Lewis, N. S. Measurement of the Free-Energy Dependence of Interfacial Charge-Transfer Rate Constants Using ZnO/H_2O Semiconductor/Liquid Contacts. *J. Am. Chem. Soc.* **2005**, *127*, 7815−7824.

DOI: 10.1021/acs.jpclett.5b00904
J. Phys. Chem. Lett. 2015, 6, 2427−2433